The Cryosphere Discuss., 9, 2397–2429, 2015
www.the-cryosphere-discuss.net/9/2397/2015/
doi:10.5194/tcd-9-2397-2015

The Cryosphere Discussions
Open Access

Temporal variations in the flow of a large Antarctic ice-stream controlled by tidally induced changes in the subglacial water system

S. H. R. Rosier[1,2], **G. H. Gudmundsson**[2], **and J. A. M. Green**[1]

[1]School of Ocean Sciences, Bangor University, Menai Bridge, LL59 5AB, UK
[2]British Antarctic Survey, High Cross, Madingley Rd., Cambridge, CB3 0ET, UK

Received: 16 March 2015 – Accepted: 23 March 2015 – Published: 15 April 2015

Correspondence to: S. H. R. Rosier (s.rosier@bangor.ac.uk)

Published by Copernicus Publications on behalf of the European Geosciences Union.

Abstract

Observations show that the flow of Rutford Ice Stream (RIS) is strongly modulated by the ocean tides, with the strongest tidal response at the 14.77 day tidal period (M_{sf}). This is striking because this period is absent in the tidal forcing. A number of mechanisms have been proposed to account for this effect, yet previous modeling studies have struggled to match the observed large amplitude and decay length scale. We use a nonlinear 3-D viscoelastic full-Stokes model of ice-stream flow to investigate this open issue. We find that the long period M_{sf} modulation of ice-stream velocity observed in data cannot be reproduced quantitatively without including a coupling between basal sliding and tidal subglacial water pressure variations. Furthermore, the subglacial water system must be highly conductive and at low effective pressure, and the relationship between sliding velocity and effective pressure highly nonlinear in order for the model results to match GPS measurements. Hydrological and basal sliding model parameters that produced a best fit to observations were a mean effective pressure $\overline{N}$ of 105 kPa, subglacial drainage system conductivity K of $7 \times 10^9\,\mathrm{m^2\,d^{-1}}$, with sliding law exponents $m = 3$ and $q = 10$. Coupled model results show the presence of tides result in a $\sim 12\,\%$ increase in mean surface velocity. Observations of tidally-induced variations in flow of ice-streams provide stronger constraints on basal sliding processes than provided by any other set of measurements.

1 Introduction

The majority of ice-streams in Antarctica are forced at their boundary by ocean tides, either directly or through the motion of an adjoining ice-shelf. Measurements have shown the flow of ice-streams to be greatly affected by ocean tides over large distances upstream from the grounding line (Anandakrishnan et al., 2003; Bindschadler et al., 2003a, b; Gudmundsson, 2006; Murray et al., 2007; Marsh et al., 2013). On Rutford Ice Stream (RIS), West Antarctica, for example, flow velocities change by more than

TCD
9, 2397–2429, 2015

10 % in response to tides over distances of 50 km upstream from the grounding line. Several different types of tidally-induced perturbations in ice flow have been observed on Antarctic ice-streams. These include stick-slip motion observed at Williams Ice Stream (Bindschadler et al., 2003a, b; Winberry et al., 2009, 2011), smooth diurnal variations observed on Kamb and Bindschadler Ice Streams (Anandakrishnan and Alley, 1997; Anandakrishnan et al., 2003), and long-periodic response found on RIS and on several other ice-streams flowing into the Ronne Ice Shelf (Gudmundsson, 2006; Murray et al., 2007; Aðalgeirsdóttir et al., 2008; King et al., 2010; Marsh et al., 2013).

An interesting aspect of the tidal observations on RIS is the long period (> 1 day) modulation in ice-stream flow that clearly demonstrates a nonlinear response to the tidal forcing (Fig. 1). In the response of the ice-stream, the dominant tidal amplitude is found at the M_{sf} tidal frequency (14.77 days), despite this tidal component being statistically insignificant in the tidal forcing. Hence, the strongest response is found at a frequency absent in the forcing. The same pattern is seen in observations of the tidal respone of other ice-streams flowing into Ronne ice-shelf (unpublised), as well as on the Larsen C ice-shelf (King et al., 2011).

One of the key motivations for studying the impact of tides on ice-stream flow is that modeling work has shown the response to reflect mechanical conditions at the glacier bed. Hence, observing and modeling tidally-induced modulations in ice-stream motion provides a window into the mechanisms that must be causing these effects.

As initially suggested by Gudmundsson (2006), a nonlinear sliding law offers a potential explanation for the RIS observations, and various flow-line and full 3-D full-Stokes models have now successfully reproduced the general aspects of the long-period modulation in ice-stream flow as arising from a nonlinear response to tidal forcing Gudmundsson (2007), King et al. (2010), Gudmundsson (2011), Walker et al. (2012), Rosier et al. (2014b). These previous studies, however, have primarily focused on identifing a potential mechanism giving rise to the observed nonlinear tidal respone on RIS by reproducing the observations qualitatively. So far, with the notable exception

TCD
9, 2397–2429, 2015

of the recent work by Thompson et al. (2014), no modeling work has attempted to replicate the RIS observations in any quantitative detail. The models presented so far have shown that the qualitative aspects of the long-period RIS response can arise through transmission of tidal stresses across the grounding line, provided the sliding law is sufficiently nonlinear. In these models the physical conditions upstream of the grounding line, as defined in these models through their sliding-law parameters, do not change with time in response to tides.

The motivation for this work are recent modeling studies that suggest that any models using time-invariant sliding-law parameters, while ignoring the effects of tidally-induced sub-glacial pressure variations on sliding, will fail to reproduce the RIS observations in quantitative terms. Recent work by Thompson et al. (2014), which does not explicitly investigate long-period modulation but includes the effects of ice-stream margins, found that for realistic ice-stream geometries, the effect of tidal stress perturbation on flow is too small to account for observations. In addition to this, our own 3-D modeling study including side drag and capable of reproducing the long period modulation, produced M_{sf} amplitudes much smaller than those observed (Rosier et al., 2014b). As a result of the discrepancies outlined above, the question as to what mechanism can lead to the observed fluctuations in surface ice velocity still remains an open one.

The first measurements of this effect made by Gudmundsson (2006), suggested M_{sf} amplitudes of ~ 0.3 m at the grounding line, decaying to ~ 0.1 m at 40 km upstream and still present at 73 km upstream. The model described by Gudmundsson (2011), although correctly producing strongest tidal response at the M_{sf} frequency, appears only to be capable of reproducing M_{sf} amplitudes of ~ 0.1 m at most. In a more recent fully 3-D study, that in contrast to Gudmundsson (2011) included lateral drag, this amplitude is decreased further to ~ 0.05 m at the grounding line when forced with the same tidal regime as that of the RIS (Rosier et al., 2014b). Hence, the observed response at the M_{sf} frequency in that model is an order of magnitude too small. Thompson et al. (2014) conclude that the observed effect is too strong to be produced by transmission of tidal stresses only and suggest that a tidally driven time-dependent

TCD
9, 2397–2429, 2015

variability in till strength through hydrological coupling could explain the observed M_{sf} response.

Here we use a 3-D nonlinear visco-elastic model with a geometry closely matching that of RIS to investigate the causes for the observed tidal response. We couple our ice-mechanical model to a model describing the changes in basal water pressure due to ocean tides, by allowing basal velocity to change in response to changes in effective basal water pressure.

The paper is organised as follows. We first describe our nonlinear visco-elastic model and present the basic govering equations. We then perform a full-Stokes surface-to-bed inversion of medial line surface velocities to determine the time averaged spatial distribution of basal sliperiness. We then establish in a thorough parameter study that the model of Rosier et al. (2014b) cannot reproduce the observed long-period velocity fluctuations of sufficient amplitude to agree with observations. In particular, and in an agreement with Thompson et al. (2014), we find that the observations can not be replicated through the effects of mechanics transmission of stresses through the ice and the till alone, but that in addition the effects of subglacial water pressure variations on sliding must be included. Finally we simulate perturbations in effective basal pressures due to ocean tides, and allow those changes in subglacial pressure to impact sliding through a commonly-used parameterisation relating sliding velocity and effective basal water pressure. After a new model parameter optimisation, we are able to replicate the RIS observations in considerable detail, but only within a fairly strict range of parameters.

TCD
9, 2397–2429, 2015

2 Methodology

2.1 Ice flow model

Our numerical ice flow model solves the field equations for conservation of mass, linear momentum (equilibrium equations) and angular momentum:

$$\frac{D\rho}{Dt} + \rho v_{i,i} = 0 \tag{1}$$

$$\sigma_{ij,j} + f_i = 0 \tag{2}$$

$$\sigma_{ij} - \sigma_{ji} = 0 \tag{3}$$

where D/Dt is the material time derivative, ρ is density, v_i are the components of the velocity vector, σ_{ij} are the components of the Cauchy stress tensor and f_i are the components of the gravity force per volume. We use the comma to denote partial derivatives and the summation convention, in line with notation commonly used in continuum mechanics. None of the terms in the equlibrium equations are omitted. In glaciology such models are commonly referred to as full-Stokes models.

We use a Maxwell rheological model that relates deviatoric stresses τ_{ij} and deviatoric strains e_{ij} with

$$\dot{e}_{ij} = \frac{1}{2G}\overset{\triangledown}{\tau}_{ij} + A\tau^{n-1}\tau_{ij}, \tag{4}$$

where A is the rate factor, the superscript $\triangledown$ denotes the upper-convected time derivative, G is the shear modulus

$$G = \frac{E}{2(1+\nu)}, \tag{5}$$

ν is the Poisson's ratio and E is the Young's Modulus. The deviatoric stresses are defined as

$$\tau_{ij} = \sigma_{ij} - \frac{1}{3}\delta_{ij}\sigma_{\mathrm{pp}}, \tag{6}$$

TCD
9, 2397–2429, 2015

and the deviatoric strains as

$$e_{ij} = \epsilon_{ij} - \frac{1}{3}\delta_{ij}\epsilon_{pp}, \tag{7}$$

where σ_{ij} and ϵ_{ij} are the stresses and strains, respectively. This rheological model approximates the visco-elastic behaviour of ice at tidal time scales, and can be thought of as a spring and dashpot in series such that the resulting strain is the sum of the elastic and viscous components and the stresses are equal.

These equations are solved using the comercial finite-element software package MSC.Marc (MARC, 2013). The ice-stream and the underlaying till are treated as two separate deformable bodies. In a previous study we have calculated the migration of the grounding line in response to ocean tides, and accounted for the resulting effect on ice flow upstream from the grounding line in a flow-line setting (Rosier et al., 2014b). Due to computational considerations we have here, however, not allowed the grounding line to migrate over tidal cycles.

Basal velocity is given by

$$\boldsymbol{u}_b = c\frac{\boldsymbol{\tau}_b^m}{N^q}, \tag{8}$$

where $\boldsymbol{\tau}_b$ is the tangential component of the basal traction, N is the effective pressure (kept constant for the initial parameter study and subsequently perturbed due to the tide), c is basal slipperiness and both m and q are exponents. The slipperiness, tangential basal traction and effective pressure are all spatially variable.

The effective subglacial water pressure N at the ice–till interface is defined as the difference between normal component of the basal traction (σ_{nn}) and the subglacial water pressure (p_w), i.e. $N = \sigma_{nn} - p_w$.

2.2 Subglacial hydrology model

Our approach to including subglacial hydrology within the finite element model framework described in Rosier et al. (2014b) is to reduce the problem to the simplest

TCD
9, 2397–2429, 2015

possible set of equations. Rather than attempt to model a complex system of connected channels and distributed flow, we treat the drainage system as a homogenous porous medium with a characteristic "conductivity" that, once coupled to the ice-flow model, can be tuned so that the velocity response matches observations. This approach to modeling subglacial hydrology has been used successfully in previous coupled studies e.g. de Fleurian et al. (2014).

As a starting point we must lay out how the tide perturbs the subglacial water pressure. We write the subglacial water pressure (p_w) at any location upstream from the grounding line as

$$p_w(x,t) = \rho_w g h(x,t) + \rho_w g(\overline{S} - b(x)), \tag{9}$$

where $h(x,t)$ is the tidally induced perturbation in the hydrological head, ρ_w is the ocean density, g the gravitational acceleration, $b(x)$ the bed elevation, and the ocean surface elevation $S(t)$ is given by

$$S(t) = \overline{S} + \Delta S(t), \tag{10}$$

where $\overline{S}$ is the mean ocean surface elevation, and $\Delta S(t)$ the ocean tide. We incorporate the effects of the tides on subglacial water pressure through the grounding-line boundary condition for the perturbation in the hydrological head h. We assume that at the grounding line the subglacial water system is in direct contact with the ocean, and the subglacial water pressure at that location is therefore equal to the ocean pressure, or

$$p_w(x,t) = \rho_w g(S(t) - b(x)) = \rho_w g(\overline{S} + \Delta S(t) - b(x)), \tag{11}$$

at $x = x_{gl}$, and hence

$$h(x_{gl},t) = \Delta S(t), \tag{12}$$

TCD
9, 2397–2429, 2015

The tidally-induced perturbation in hydrological head is then modelled as a diffusion process, i.e.

$$\partial_t h = K\,\partial^2_{xx} h, \tag{13}$$

where K is the hydraulic conductivity. In the context of Darcy groundwater flow, K can be expressed as

$$K = \frac{\rho_w g k}{\mu} S_s, \tag{14}$$

where k is the permeability, μ the viscosity of water, and S_s the specific storage capacity. In reality this parameter combination is poorly constrainted and here treated as an unknown.

Thus our approach is to solve for tidal perturbations in hydraulic head (rather than water pressure) which is known at the grounding line and transmitted upstream through a simple diffusion process controlled by the conductivity K. When modeling the spatial and the temporal variations of the subglacial drainage system water, we only attempt to describe the perturbations in effective pressure due to tides. This avoids the complications of calculating the temporally-averaged pressure field, which is unnecessary as the effects of the mean pressure on basal flow are already accounted for in the temporally averaged value of the basal slipperiness which we derive in our inversion (see below).

This is coupled to our ice-stream model through the sliding law (Eq. 8) which we expand to consider perturbations in N:

$$\boldsymbol{u}_b = c\frac{\boldsymbol{\tau}_b^m}{(\overline{N} + \Delta N)^q} \tag{15}$$

where

$$\Delta N = -\rho_w g h(x,t) \tag{16}$$

TCD
9, 2397–2429, 2015

and $\overline{N}$ is mean effective pressure such that $N = \overline{N} + \Delta N$. Re-arranging this gives

$$\boldsymbol{u}_b = c' \frac{\boldsymbol{\tau}_b^m}{(1+\xi)^q}, \tag{17}$$

where $c' = c\overline{N}^{-q}$ and $\xi = \Delta N/\overline{N}$. This now puts slipperiness and mean effective pressure into a new c' term which is a function of x but not a function of t. In this way the baseline effective pressure and slipperiness conditions that affect the mean velocity of the glacier are separated from the perturbed terms. The c' term is what is inverted for, as described later, to match observed medial line flow. Re-arranging the equation in this way means that $\overline{N}$ only affects the relative size of the non-dimensionalised perturbation ξ and not the mean flow which is constrained by observations.

The hydrological coupling leads to six constants: $\overline{N}$, K, ν, E, m and q which are treated as unknowns. The rheological parameters E (Young's modulus) and ν (Poisson's ratio) are constrained to some extent from previous visco-elastic modeling efforts on tidally induced motion, with values of E expected to be ~ 4.8 GPa and ν of ~ 0.41 (Reeh et al., 2003; Gudmundsson, 2011). The sliding law exponents m and q are treated here as tunable parameters. Note that once c' has been determined, through the inversion procedure outlined below, K and $\overline{N}$ only affect modeled flow through their combined effect on ξ. Sensitivity of the model to the choice of these parameters is presented later.

2.3 Model geometry

Our model geometry is based on the RIS, however, we have not attempted to reproduce its geometry exactly and our thickness distribution in along-flow direction corresponds to the mean ice thickness across the ice-stream. The 3-D model domain (Fig. 2) has zero bed slope, a surface slope of 0.0036 and ice thickness at the grounding line of 2040 m. While using constant slopes is a simplification and in reality the bed

TCD
9, 2397–2429, 2015

undulates considerably over the 100 km length being considered, there is no obvious overall shallowing or deepening, and the surface slope is relatively uniform. The width and length of the model domain are 16 and 120 km, respectively. The hydrological component of the model extends a further 100 km upstream.

2.4 Boundary conditions

A no-slip condition is applied along one of the lateral boundaries and a free-slip condition along the other. The latter represents the ice stream medial line, giving an overall width of 32 km for the symmetrical problem approximately matching that of the RIS. Along the upper in-flow boundary, a surface traction is prescribed based on the analytical solution for the flow of a uniformly-inclined slap of ice. At the downstream boundary, a surface traction is prescribed based on the analytical solution for the flow of an ice shelf in one horizontal dimension, i.e.

$$\sigma_{xx} = -\rho_i g(s-z) + \frac{\rho_i g H}{2}\left(1 - \frac{\rho_i}{\rho_w}\right) - p_b, \tag{18}$$

where ρ_i and ρ_w are ice and water density respectively (910 and 1030 kg m^{-3}), H is the ice thickness, s is the ice surface, z is the depth, g is gravitational acceleration and p_b is a "backpressure" term that we treat as unknown and include in the inversion. In the case of the RIS, a non-zero value of p_b could, for example, be expected to result from lateral resistance to ice-shelf flow.

Two boundary conditions are necessary to solve for the diffusion of hydraulic head upstream from the grounding line. As mentioned earlier, at $x = x_{gl}$ subglacial water pressure and ocean pressure are assumed to be equal, leading to the boundary condition given in Eq. (12). At the upstream boundary the condition $h \to 0$ as $x \to \infty$ is strictly correct for this form of diffusion equation. Since this is not possible to implement in our model we use $h = 0$ at $x = 200$ km, assuming that h is very small at the upstream boundary. This can be justified analytically by solving Eq. (13) to give a decay length

TCD
9, 2397–2429, 2015

scale, for some periodic change in hydraulic head, of $\sqrt{2K/\omega}$ where ω is the tidal angular frequency being considered. For the range of conductivity values and tidal frequencies considered here, the model domain of 200 km is far larger than this length scale, thus this boundary condition can be safely applied without influencing the model results.

Ocean pressure is applied to the base of the floating ice-shelf as a spring foundation and the tidal forcing is introduced into the model as a perturbation in mean sea level. The tidal forcing is taken from the CATS2008 tidal model output (Padman et al., 2008), using the largest six tidal constituents at the RIS grounding line (M_2, S_2, O_1, K_1, K_2 and N_2).

2.5 Model initialisation

Preliminary experiments were conducted in which the stress exponent of the flow law (m) was changed to examine the effect on M_{sf} response. Changing this parameter alters the mean flow in a non-trivial way that cannot be simply accounted for by altering slipperiness over the entire domain. Since the M_{sf} response is sensitive to mean velocity it is important when comparing results to keep the mean velocity as close to observations as possible. To reproduce the general pattern of observed surface velocities on RIS, and in particular the general increase in velocities towards the grounding line, we invert for slipperines (c') using the medial line velocities (note the term slipperiness here encompasses bed slipperiness and mean effective pressure).

A Bayesian inversion approach was used to empirically calculate the $i \times j$ sensitivity matrix **K** describing the sensitivity of surface velocities to basal slipperiness. The method and equations are broadly similar to those presented in Raymond and Gudmundsson (2009) except that, rather than using analytical expressions for the sensitivity matrix, it is computed as the partial derivative of the forward model with

TCD
9, 2397–2429, 2015

respect to the state vector. The sensitivity matrix is given by

$$[\mathbf{K}]_{pq} = \frac{\partial \boldsymbol{u}_p}{\partial c'_q}, \tag{19}$$

where p and q are nodal numbers along the upper and lower surfaces of the finite element mesh. Here the measurement vector $\boldsymbol{u}$ has i elements and is the surface velocity, and the state vector c' has j elements and is the slipperiness at the bed. Thus we calculate, for each element of the state vector, the change in measurement vector, giving one entire column of $\mathbf{K}$. This is repeated for every element of the state vector to build up a complete sensitivity matrix.

Since the model response to a change in slipperiness is nonlinear, the inversion will not converge to an optimum solution in a single iteration and so a Newton–Gauss iterative approach is used of the form

$$c'_{i+1} = c'_i + \hat{\mathbf{S}}^{-1}\left(\mathbf{K}_i^T \mathbf{S}_\mathrm{e}^{-1}\left[\boldsymbol{u} - \mathbf{F}(c'_i)\right] - \mathbf{S}_\mathrm{a}^{-1}\left[c'_i - c'_\mathrm{a}\right]\right), \tag{20}$$

where

$$\hat{\mathbf{S}}^{-1} = \mathbf{K}_i^T \mathbf{S}_\mathrm{e}^{-1} \mathbf{K}_i + \mathbf{S}_\mathrm{a}^{-1} \tag{21}$$

is the Fisher information matrix, $\mathbf{S}_\mathrm{e}$ is the covariance of measurement errors, $\mathbf{S}_\mathrm{a}$ is the covariance of a priori errors and $\mathbf{F}(c')$ is the forward model (Rodgers, 2000). Measurement errors (σ_e) are assumed to be uncorrelated and have a normal distribution, such that the measurement error covariance matrix is proportional to the identity matrix, in the form $\mathbf{S}_\mathrm{e} = \sigma_\mathrm{e}^2 \mathbf{I}_\mathrm{m}$.

Our treatment of the prior covariance matrix is the same as Gudmundsson and Raymond (2008), based on the assumption that basal slipperiness is spatially correlated, whereby each prior estimate of c' at location i is related to a neighbouring location $i-1$ by

$$c'_i = \phi_c c'_{i-1} + \epsilon_c \tag{22}$$

TCD
9, 2397–2429, 2015

where ϵ_c has variance σ^2. The elements of $\mathbf{S}_a^{-1}$ can then be given by

$$[\mathbf{S}_a]_{pq} = \sigma_a^2 \, e^{-|p-q|/\lambda}, \tag{23}$$

where λ is a decay length scale, related to ϕ_c by $\lambda = -1/\ln \phi_c$ and the variance is

$$\sigma_c^2 = \frac{\sigma^2}{1-\phi_c^2}. \tag{24}$$

This results in a covariance matrix which has σ_a^2 along the diagonal and non-zero off-diagonal elements.

We reduce the number of calculations needed by only taking into account along-flow variations in slipperiness. Since we only invert for the medial line velocity and the geometry we use is idealised this simplification is valid. Buttressing (p_b, which is particularly relevant for flow velocities near the grounding line) is inverted for by adding a single non-dimensionalised element to the end of the state vector. This is treated in the same way as the other state vector elements apart from having its own (uncorrelated) prior error estimate.

Although this "brute force" approach to inverting for basal slipperiness is computationally more expensive than others such as the adjoint method, there are a number of advantages of this method such as giving an explicit estimate of the inversion error. Furthermore, because each element of the **K** matrix is independent of all the others, it is possible to easily parallelize its calculation, meaning that run times need not be orders of magnitude greater if sufficient computing resources are available. The sensitivity matrix need not be calculated for each iteration and in fact it is advantageous to iterate a number of times using the same matrix before re-calculating it. The iteration was continued until it converged on the maximum a posteriori solution, in contrast to many other similar studies which stop iterating once the misfit between model output and observations is below a given threshold.

TCD
9, 2397–2429, 2015

3 Results

As discussed above, to date no model has been presented that matches the RIS tidal observations. Admittedly, most models have focused on trying to identify the mechamism responible for the rather striking observation that the response of the ice-stream is concentrated at tidal frequencies absent in the forcing. However, it would be expected that if the mechanism has been correctly identified, and is the primary cause for the velocity fluctuations, modeled amplitudes would be close to those measured. In fact modeling work presented so far has always produced too small a response at the M_{sf} tidal period, and too strong at both diurnal and semi-diurnal periods.

3.1 Modeling the tidal response of RIS assuming no temporal changes in water pressure

To address the open question of whether RIS observations can be replicated through stress transmission alone, our first modeling aim is to establish an upper bound on the possible M_{sf} amplitude in the absense of any temporal changes in bed conditions, i.e. other than those resulting from direct stress transmission through the ice due to the flexing of the ice in response to tides. In the context of our modeling methodolgy described above this is equal to setting the stress exponent, q, of the effective water pressure in the sliding law (see Eq. 8) to zero. In effect we repeat the fully 3-D simulations conducted in Rosier et al. (2014b) but with a broader range of parameters, an ice-stream geometry closer to that of RIS and a basal slipperiness distribution ($c(x)$) determined through a formal inversion of surface velocities. Our tunable model parameters with no subglacial hydrological coupling are: the Poisson's ratio (ν), the Young's modulus (E), and the stress exponent (m). We set the stress exponent (n) in Glen's flow law to $n = 3$, and determine the rate factor A from a static temperature distribution defined in the model using the commonly used temperature relation given by Hutter (1983).

TCD
9, 2397–2429, 2015

We performed an extensive parameter study. For every value of the basal sliding-law stress exponent m, we first determined the maximum a posteriori distribution of basal slipperiness (c') using our inversion approach. In the surface-to-bed inversion the long-term average flow in the absence of tidal forcing was matched to the observed velocity, and a (purely) viscous flow model was therefore used in the forward step. We then forced our visco-elastic time-dependent model by tides. For each given value of m and the associated basal slipperiness distribution, tidal response was calculated for a range of elastic rheology parameters. From modelled horizontal displacements curves, we then calculated tidal amplitudes and phases as a function of distance along the medial line. By fitting an exponential curve to the spatial variation in tidal amplitudes, we then determined decay length scales for each tidal component, as well as phase velocities. We varied the stress exponent m from 1 to 10, and the Young's modulus from 1 to 6 GPa. The Poisson's ratio was varied between 0.3 and 0.45, but was found to have almost no effect on the modelled tidal response and we do not discuss those results further.

The results of the parameter study are summarized in Fig. 4. In Fig. 4a the amplitude of the M_{sf} frequency 10 km upstream from the grounding line is shown. The modelled M_{sf} amplitudes are never larger than a few centimeters. The largest values are found for high m and high E values. Although somewhat higher M_{sf} amplitudes could be obtained by increasing m even further, the modelled results show that this increase is sub-linear as a funciton of m. Furthermore, for $m > 10$ other model outputs that must match observations such as phase velocity, decay length scale and notably M_2 amplitude, would also increase beyond the range of desired values. The model is, thus, not able to reproduce the observed magnitude of the M_{sf} tidal amplitude.

Both the decay length scale (Fig. 4c) and phase velocity (Fig. 4d) increase with increasing m, in agreement with the analytical solution derived in previous work (Rosier et al., 2014b).

The amount of buttressing needed to match observed velocities increases as m is increased and varied from 650 to 850 KPa for $m = 1$ to 10 (note that the inversion

TCD
9, 2397–2429, 2015

procedure, in minimising the cost function, tries to find a solution that does not vary significantly from the a priori estimates of slipperiness and buttressing, and therefore this buttressing value may be to some extent artificial if the a priori buttressing estimate and error are poorly chosen).

Decay of the M_{sf} amplitude upstream of the grounding line for all parameter study simulations is plotted in Fig. 5 (blue lines) and compared with the observed amplitudes (crosses). This clearly shows the disparity between desired amplitude and the range of possible amplitudes using the mechanism described above. The conclusion from this parameter study, in agreement with Thompson et al. (2014), is that stress transmission alone cannot explain the large amplitude of M_{sf} modulation, with maximum amplitudes 10 km upstream approaching ~ 0.05 m, considerably smaller than the desired 0.3 m. Clearly an additional nonlinear effect is needed to match observations. Although stress-transmission can reproduce the qualitative aspects of the data, in particular the generation of M_{sf} response, the effects are (at the most) about an order-of magnitude smaller than revealed by measurements.

3.2 Modeling the tidal response of RIS assuming temporal changes in water pressure

We now couple our hydrological model (Sect. 2.2) to the 3-D full-Stokes model by using values of $q > 0$ in order to see whether this can explain measurements made on the RIS.

Coupled model results obtained through optimization of hydrological parameters are shown in Fig. 6. This provides a much better agreement with GPS measurements than any previous combination of parameters for the model with no subglacial water pressure coupling. Notably, the M_{sf} amplitude and decay length scale are both large and match very closely with data (Fig. 5). The hydrological model used a mean effective pressure ($\overline{N}$) of 105 kPa, pressure exponent (q) of 10 and conductivity (K) of 7×10^9 m^2 d^{-1}. Other model parameters were $E = 4.8$ GPa, $\nu = 0.41$ (both in accordance with the optimum Maxwell rheology given by Gudmundsson, 2011) and $m = 3$. The

TCD
9, 2397–2429, 2015

only feature of these results that is arguably not in agreement with observations is the amplitude of the semi-diurnal tidal constituent detrended displacements. Comparison between Figs. 1 and 6 shows an M_2 amplitude that is approximately twice as large at the grounding line as the amplitude determined by tidal analysis of the data. Possible explanations for this are that the M_2 amplitude is too small to be sufficiently resolved by the GPS receivers that originally made the measurements or limitations of the simple Maxwell rheology.

We perform a sensitivity analysis to determine whether the M_{sf} response is robust or highly sensitive to certain parameters. Figure 7 shows change in M_{sf} amplitude (panel a), M_2 amplitude (panel b), M_{sf} decay length scale (panel c) and M_{sf} phase velocity (panel d) compared to the optimised model for a ±10 % change in each parameter. Comparison of panels a and b in Fig. 7 suggest that the calculated M_{sf} and M_2 amplitudes are closely correlated and thus, for the parameters tested here, there is no clear modification of the model that would decrease the semidiurnal (M_2) amplitude without also reducing the M_{sf} response. Softening the ice by reducing E may be one possible route, since this appears to increase M_{sf} amplitude more than M_2 amplitude, however this parameter is more tightly constrained than others since the rheology of ice is not entirely unknown and the sensitivity is too small to solve the issue. M_{sf} amplitude is most sensitive to normalized changes in $\overline{N}$ and q, as might be expected since it is the nonlinearity here that drives the majority of the long period modulation in flow.

A reduction in m increases the nonlinear response of the modeled ice-stream, the reverse of the response with no hydrological coupling, but increases the M_{sf} length scale and phase velocity. Overall, all parameters are most sensitive to the choice in $\overline{N}$. This is not surprising, since ΔN is small then as $\overline{N}$ gets large the dimensionless number ξ will drop out and that source of nonlinearity disappears.

The large difference in M_{sf} amplitude between the parameter study simulations and those that include tidally induced subglacial pressure variation poses an important question; is a nonlinear sliding law where $m > 1$ required at all, given that the M_{sf} modulation appears to be largely generated by water pressure changes. Results

TCD
9, 2397–2429, 2015

from the sensitivity analysis suggest that the stress exponent m remains a crucial parameter in altering characteristics of the M_{sf} response. To look at this in more detail, the model was re-run with varying exponents q and m, with the aim of examining the characteristics of the M_{sf} response given changes in the dominance of the two mechanisms.

The four characteristics of the model's tidal response are plotted against exponents q and m, each varying between 1 and 10, in Fig. 8. These results show that reducing m leads to an increase in amplitude of both tidal frequencies investigated, but a decrease in the length scale and phase velocity. An M_{sf} decay length scale of ~ 50 km is observed on the RIS but panel c shows that for $m = 1$ the length scale is smaller up to $q = 10$ and in fact appears to have reached an asymptote. Increasing m for any given value of q however leads to a large increase in the length scale. The mechanism by which increasing m reduces M_{sf} amplitude but increases length scale is discussed later but suggests that a flow low with $m > 1$ is still required to reproduce the RIS tidal response.

4 Discussion

We find that stress transmission alone cannot fully explain the observed M_{sf} modulation of surface velocities on the RIS. An additional mechanism whereby a tidally induced pressure wave travels up a subglacial drainage system, altering the effective pressure at the base of the ice-stream, is required to produce a sufficiently large M_{sf} amplitude. The drainage system must be highly conductive and sufficiently nonlinear, such that a small change in basal water pressure leads to a large change in surface velocity.

This nonlinearity arises largely in two of the parameters: $\overline{N}$ and q. The model does not take into account feedbacks between ice flexure and water pressure. Tidal flexure causes changes in normal stress which would perturb the subglacial water pressure and it has been suggested that this mechanism could "pump" brackish water upstream (Walker et al., 2013; Sayag and Worster, 2013). This flexure may have the additional effect of opening crevasses beneath the ice or dilating the subglacial till, leading to

TCD
9, 2397–2429, 2015

changes in local water storage and thereby altering the distribution of water. Our justification in ignoring these additional processes is that ice flexure is limited to within several ice thicknesses of the grounding line and the M_{sf} modulation is observed to travel much further upstream.

Spatial variations in $\overline{N}$ are accounted for in the inverted c' and cannot be separated from spatial variability in c. In reality if $\overline{N}$ varied spatially this would affect the nonlinearity in ξ. Ultimately we ignore this additional complication and the decay in ξ is only a function of the spatially uniform conductivity, K. In doing so several processes are combined to provide a more general picture of the subglacial drainage characteristics. A fit to observations could to some extent still be obtained if $\overline{N}$ was altered by compensating with a change in q since the two parameters are correlated. In general though, a relatively low value of effective pressure with no large gradient going upstream from the grounding line is needed, since a gradient would cause the nonlinearity to be rapidly reduced in the upstream direction.

In order to understand the interaction between the hydrology and stress transmission mechanisms it is important to consider the relative timing with which they act on the ice-stream. As explained previously, an exponent $m > 1$ causes an increase in ice velocity during low tide and decrease at high tide. Conversely, at high tide near the grounding line the water pressure within the subglacial drainage system will be at its highest, lowering the effective pressure and increasing ice velocity. The two effects are therefore opposite in phase at the grounding line (although in both cases the peak velocities are still during the spring tide, so there is no phase shift in the M_{sf} frequency that they generate at this point). Since the subglacial pressure effect is larger it dominates at the grounding line and the reduction in M_{sf} amplitude at this point for $m > 1$ is a result of the stress transmission effect being 180° out of phase with the subglacial pressure variations, thereby dampening the velocity modulation.

Results from Fig. 8 suggest that, while it may be possible to reproduce the observed M_{sf} response of the RIS for $m = 1$, this would necessitate an almost infinite conductivity in order to transmit the signal far enough upstream. With the set of model parameters

TCD
9, 2397–2429, 2015

presented, the effect of subglacial pressure variations dominates at the grounding line and can produce very large M_{sf} amplitudes, but what is much more difficult is to reproduce the long decay length scale of this frequency. The key parameter then becomes m, which can substantially increase the decay length scale given values $m > 1$. Any reduction in the M_{sf} amplitude from using a high value of m can be compensated for by increasing the nonlinearity of the drainage system (reducing $\overline{N}$ or increasing q).

None of the other parameters within the model had such a large effect on the length scale and the implication is that a nonlinear sliding law is required in addition to any nonlinear response to subglacial pressure variations. Matching the observed long period modulation of ice-stream flow requires a balance between large M_{sf} amplitude and decay length scale. A choice of m that is too small means the M_{sf} signal will decay too rapidly upstream of the grounding line, but too large and the generation of the signal due to subglacial hydrology becomes hindered.

An explanation for this increase in length scale with $m > 1$ can be thought of intuitively as follows. Consider the propogation of nonlinear M_{sf} period up the RIS as two waves, generated by the upper and lower terms on the right of Eq. (8). These two waves clearly have the same frequency but since they propogate up the ice-stream by different mechanisms it is reasonable to assume they have different phase velocities. At x_{gl} they are 180° out of phase but with different phase speeds this destructive interference becomes constructive interference as you move away from the source. As a consequence the M_{sf} amplitude is reduced at the grounding line but it's decay may be slowed as a result of constructive interference upstream.

The requirement of high conductivity in order to transmit the tidal signal far enough upstream to match observations suggests that there must be a channelized drainage system beneath the RIS. This could consist of a few large channels that transmit the tidal pressure wave far upstream which then permeates through the till on either side of the channel, leading to changes in effective pressure over large portions of the ice-stream base.

TCD
9, 2397–2429, 2015

Gudmundsson (2011) demonstrated that the nonlinearity described above leads to an increase in the RIS mean velocity of ∼ 5 % due to the presence of the tides. A simulation with identical model setup to that used in Fig. 6 but with tidal amplitude set to zero everywhere was done to examine this process with the larger M_{sf} amplitudes presented in this work. The result with this new model, that successfully replicates the amplitude of long period modulation, is that mean surface velocity is increased by ∼ 12 % due to the presence of the tides. This is a considerable increase on the previous value which is expected since the M_{sf} amplitudes in that model were smaller. It demonstrates that tidal forcing can not necessarily be ignored over longer time scales. Future changes in ice-shelf thickness and extent could lead to interesting feedbacks between tidal amplitudes and ice-stream velocities (Rosier et al., 2014a).

5 Conclusions

Obervations of surface motion of the RIS show a strong, nonlinear response that propogates a long way upstream from the grounding line. The nonlinear response of this ice-stream and others in the region is striking both in its amplitude and extent and matching observations is not possible through stress transmission considerations alone. Coupling with a hydrological model that sends tidally-induced subglacial pressure variations far upstream is required to explain these observations. Furthermore, three other requirements must be met; low effective pressure across the entire ice-stream bed, a highly conductive subglacial drainage system and a nonlinear sliding law such that $m > 1$.

Hydrological and basal sliding model parameters that produced a best fit to observations were $m = 3$, $q = 10$, $K = 7 \times 10^9\,\mathrm{m^2\,d^{-1}}$ and $\overline{N} = 105\,\mathrm{kPa}$. Although a complete exploration of the parameter space is not currently possible due to prohibitive computational expense, we are confident that the set of parameters outlined above is robust for our simplified 3-D model. Future models, incorporating detailed RIS topography, could further constrain these parameters. We know of no other approach

TCD
9, 2397–2429, 2015

that can provide these insights into the controls on basal motion. Our conclusion from attempting to match the observed nonlinear response of the RIS is that a channelized and highly efficient drainage system must exist at the bed in order to reproduce an M_{sf} response of sufficient amplitude and extent.

Acknowledgements. We thank J. Kingslake, Jan De Rydt and C. Martin for their comments on the manuscript and many helpful suggestions during the course of this work. This study is part of the British Antarctic Survey Polar Science for Planet Earth Programme. Funding was provided by the UK Natural Environment Research Council through grants NE/J/500203/1 (SHRR PhD studentship) and NE/F014821/1 (JAMG Advanced Fellowship).

References

Aðalgeirsdóttir, G., Smith, A. M., Murray, T., King, M. A., Makinson, K., Nicholls, K. W., and Behar, A. E.: Tidal influence on Rutford Ice Stream, West Antarctica: observations of surface flow and basal processes from closely-spaced GPS and passive seismic stations, J. Glaciol., 54, 715–724, doi:10.3189/002214308786570872, 2008. 2399

Anandakrishnan, S. and Alley, R.: Tidal forcing of basal seismicity of ice stream C, West Antarctica, observed far inland, J. Geophys. Res., 102, 15183–15196, doi:10.1029/97JB01073, 1997. 2399

Anandakrishnan, S., Voigt, D. E., and Alley, R. B.: Ice stream D flow speed is strongly modulated by the tide beneath the Ross Ice Shelf, Geophys. Res. Lett., 30, 1361, doi:10.1029/2002GL016329, 2003. 2398, 2399

Bindschadler, R. A., King, M. A., Alley, R. B., Anandakrishnan, S., and Padman, L.: Tidally controlled stick-slip discharge of a West Antasrctic ice stream, Science, 301, 1087–1089, doi:10.1126/science.1087231, 2003a. 2398, 2399

Bindschadler, R. A., Vornberger, P. L., King, M. A., and Padman, L.: Tidally driven stickslip motion in the mouth of Whillans Ice Stream, Antarctica, Ann. Glaciol., 36, 263–272, doi:10.3189/172756403781816284, 2003b. 2398, 2399

Cuffey, K. M. and Patterson, W. S. B.: The Physics of Glaciers, 4th edn., Butterworth-Heineman, 30 Corporate Drive, Suite 400, Burlington, MA 01803, USA, 2010.

TCD
9, 2397–2429, 2015

de Fleurian, B., Gagliardini, O., Zwinger, T., Durand, G., Le Meur, E., Mair, D., and Råback, P.: A double continuum hydrological model for glacier applications, The Cryosphere, 8, 137–153, doi:10.5194/tc-8-137-2014, 2014. 2404

Gudmundsson, G. H.: Fortnightly variations in the flow velocity of Rutford Ice Stream, West Antarctica, Nature, 444, 1063–4, doi:10.1038/nature05430, 2006. 2398, 2399, 2400

Gudmundsson, G. H.: Tides and the flow of Rutford Ice Stream, West Antarctica, J. Geophys. Res., 112, F04007, doi:10.1029/2006JF000731, 2007. 2399

Gudmundsson, G. H.: Ice-stream response to ocean tides and the form of the basal sliding law, The Cryosphere, 5, 259–270, doi:10.5194/tc-5-259-2011, 2011. 2399, 2400, 2406, 2413, 2418

Gudmundsson, G. H. and Raymond, M.: On the limit to resolution and information on basal properties obtainable from surface data on ice streams, The Cryosphere, 2, 167–178, doi:10.5194/tc-2-167-2008, 2008. 2409

Hutter, K.: Theoretical glaciology, in: Mathematical Approaches to Geophysics, Vol. 1, Springer Netherlands, 1983. 2411

King, M. A., Murray, T., and Smith, A. M.: Non-linear responses of Rutford Ice Stream, Antarctica, to semi-diurnal and diurnal tidal forcing, J. Glaciol., 56, 167–176, doi:10.3189/002214310791190848, 2010. 2399

King, M. A., Makinson, K., and Gudmundsson, G. H.: Nonlinear interaction between ocean tides and the Larsen C Ice Shelf system, Geophys. Res. Lett., 38, 1–5, doi:10.1029/2011GL046680, 2011. 2399

MARC: Marc users manual, MSC Software Corporation, 2 MacArthur Place, Santa Ana, CA 92707, USA, 2013. 2403

Marsh, O. J., Rack, W., Floricioiu, D., Golledge, N. R., and Lawson, W.: Tidally induced velocity variations of the Beardmore Glacier, Antarctica, and their representation in satellite measurements of ice velocity, The Cryosphere, 7, 1375–1384, doi:10.5194/tc-7-1375-2013, 2013. 2398, 2399

Murray, T., Smith, A. M., King, M. A., and Weedon, G. P.: Ice flow modulated by tides at up to annual periods at Rutford Ice Stream, West Antarctica, Geophys. Res. Lett., 34, 6–11, doi:10.1029/2007GL031207, 2007. 2398, 2399

Padman, L., Erofeeva, S. Y., and Fricker, H. A.: Improving Antarctic tide models by assimilation of ICESat laser altimetry over ice shelves, Geophys. Res. Lett., 35, L22504, doi:10.1029/2008gl035592, 2008. 2408

TCD
9, 2397–2429, 2015

Raymond, M. J. and Gudmundsson, G. H.: Estimating basal properties of ice streams from surface measurements: a non-linear Bayesian inverse approach applied to synthetic data, The Cryosphere, 3, 265–278, doi:10.5194/tc-3-265-2009, 2009. 2408

Reeh, N., Christensen, E. L., Mayer, C., and Olesen, O. B.: Tidal bending of glaciers: a linear viscoelastic approach, Ann. Glaciol., 37, 83–89, doi:10.3189/172756403781815663, 2003. 2406

Rodgers, C. D.: Inverse Methods for Atmospheric Sounding: Theory and Practice, World Scientific Publishing, 57 Shelton street, Covent garden, London, WC2H 9HE, 2000. 2409

Rosier, S. H. R., Green, J. A. M., Scourse, J. D., and Winkelmann, R.: Modeling Antarctic tides in response to ice shelf thinning and retreat., J. Geophys. Res.-Oceans, 119, 87–97, doi:10.1002/2013JC009240, 2014a. 2418

Rosier, S. H. R., Gudmundsson, G. H., and Green, J. A. M.: Insights into ice stream dynamics through modelling their response to tidal forcing, The Cryosphere, 8, 1763–1775, doi:10.5194/tc-8-1763-2014, 2014b. 2399, 2400, 2401, 2403, 2411, 2412

Sayag, R. and Worster, M. G.: Elastic dynamics and tidal migration of grounding lines modify subglacial lubrication and melting, Geophys. Res. Lett., 40, 5877–5881, doi:10.1002/2013GL057942, 2013. 2415

Thompson, J., Simons, M., and Tsai, V. C.: Modeling the elastic transmission of tidal stresses to great distances inland in channelized ice streams, The Cryosphere, 8, 2007–2029, doi:10.5194/tc-8-2007-2014, 2014. 2400, 2401, 2413

Walker, R. T., Christianson, K., Parizek, B. R., Anandakrishnan, S., and Alley, R. B.: A viscoelastic flowline model applied to tidal forcing of Bindschadler Ice Stream, West Antarctica, Earth Planet. Sc. Lett., 319–320, 128–132, doi:10.1016/j.epsl.2011.12.019, 2012. 2399

Walker, R. T., Parizek, B. R., Alley, R. B., Anandakrishnan, S., Riverman, K. L., and Christianson, K.: Ice-shelf tidal flexure and subglacial pressure variations, Earth Planet. Sc. Lett., 361, 422–428, doi:10.1016/j.epsl.2012.11.008, 2013. 2415

Winberry, J. P., Anandakrishnan, S., Alley, R. B., Bindschadler, R., and King, M. A.: Basal mechanics of ice streams: Insights from the stick-slip motion of Whillans Ice Stream, West Antarctica, J. Geophys. Res., 114, F01016, doi:10.1029/2008JF001035, 2009. 2399

Winberry, J. P., Anandakrishnan, S., Wiens, D. A., Alley, R. B., and Christianson, K.: Dynamics of stick-slip motion, Whillans Ice Stream, Antarctica, Earth Planet. Sc. Lett., 305, 283–289, doi:10.1016/j.epsl.2011.02.052, 2011. 2399

TCD
9, 2397–2429, 2015

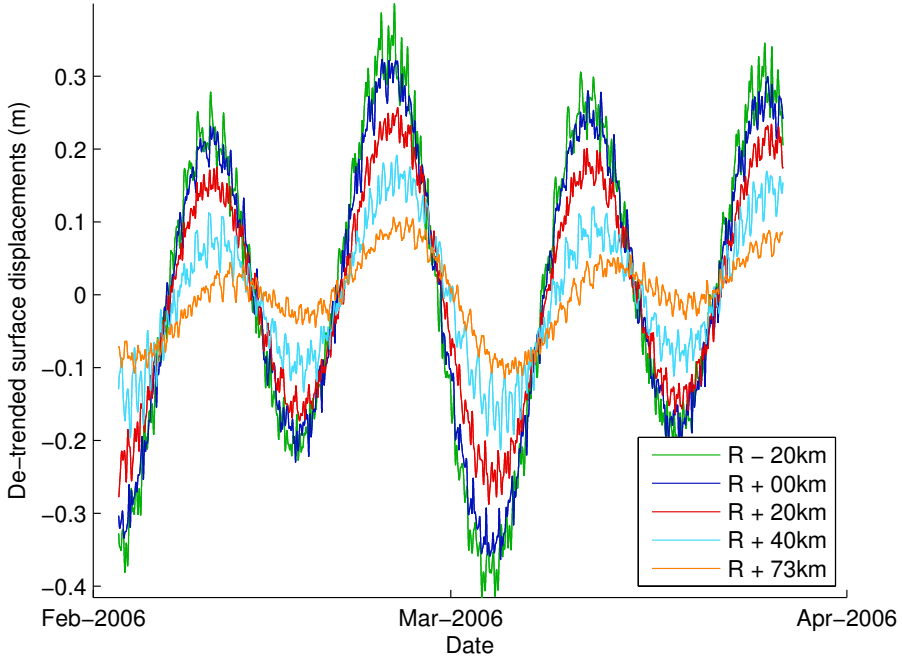

Figure 1. Linearly detrended horizontal displacements on the RIS reproduced by a tidal fit to the original measured data. Measurements are shown from five GPS stations at 20 km downstream of the grounding line ($R - 20$ km), at the grounding line ($R + 00$ km) and distances of 20, 40 and 73 km upstream from the grounding line ($R + 20$, $R + 40$ and $R + 73$ km respectively).

TCD
9, 2397–2429, 2015

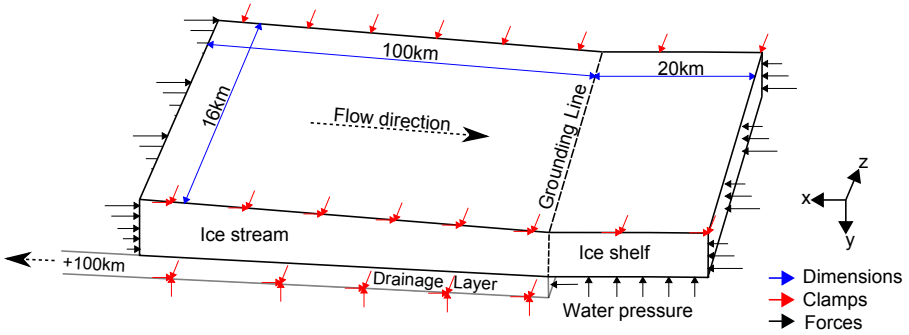

Figure 2. 3-D model domain, showing the boundary forces (black arrows) and flow constraints (red arrows). The subglacial drainage system extends a further 100 km upstream from the ice-stream boundary. Note that since the problem is symmetrical, the medial line is considered to be the plane $z = 0$ and the ice-stream being modelled is therefore 32 km wide.

TCD
9, 2397–2429, 2015

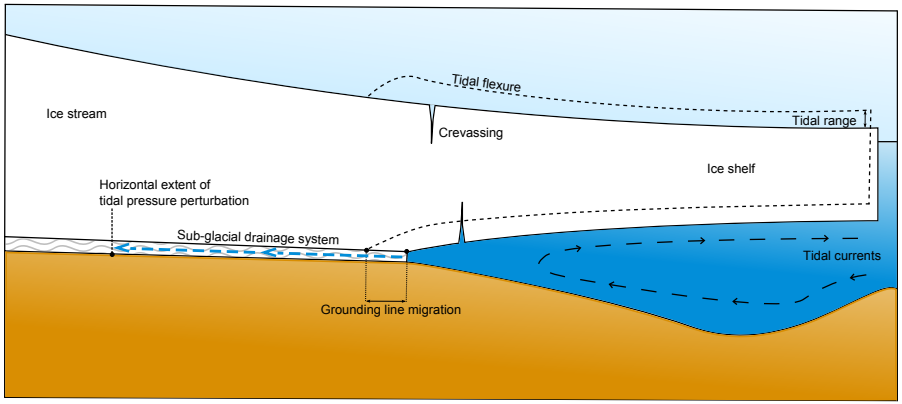

Figure 3. Schematic showing the various mechanisms by which tides can influence ice-stream flow.

TCD
9, 2397–2429, 2015

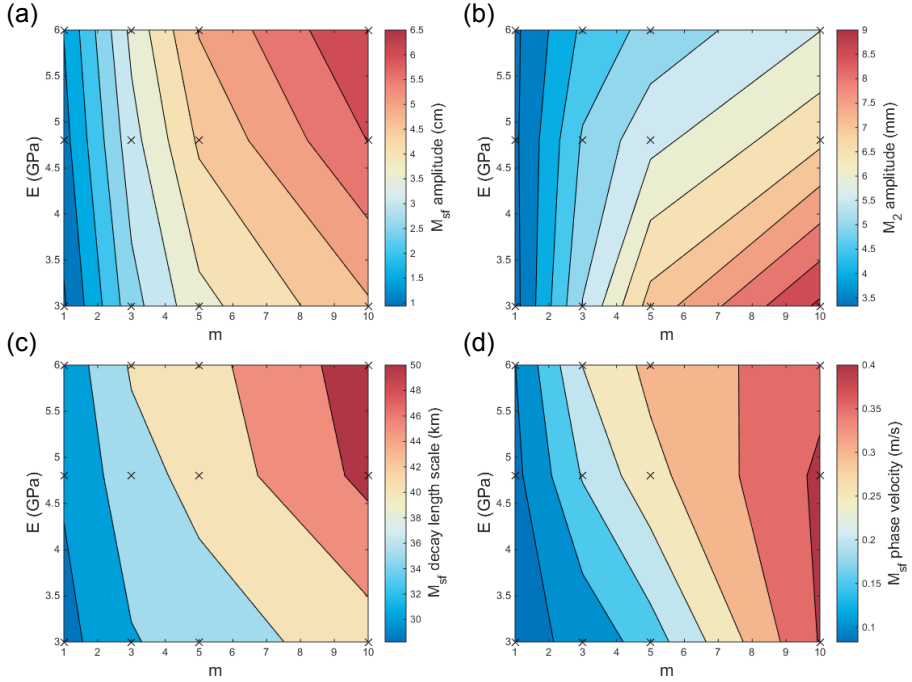

Figure 4. Modelled M_{sf} and M_2 tidal amplitudes 10 km upstream from the grounding line (upper left and upper right panels, respectively), and M_{sf} decay lenght scales and phase velocities (lower left and lower right panels, respectivily) as a funciton of the basal sliding law stress exponent m and the elastic Young's modulus of ice. Here the potential effects of subglacial water pressure variations in response to tides on sliding were not included, i.e. in the sliding law (Eq. 8), $q = 0$. Crosses indicate model simulations. The contour plot is based an interpolatin of model results.

TCD
9, 2397–2429, 2015

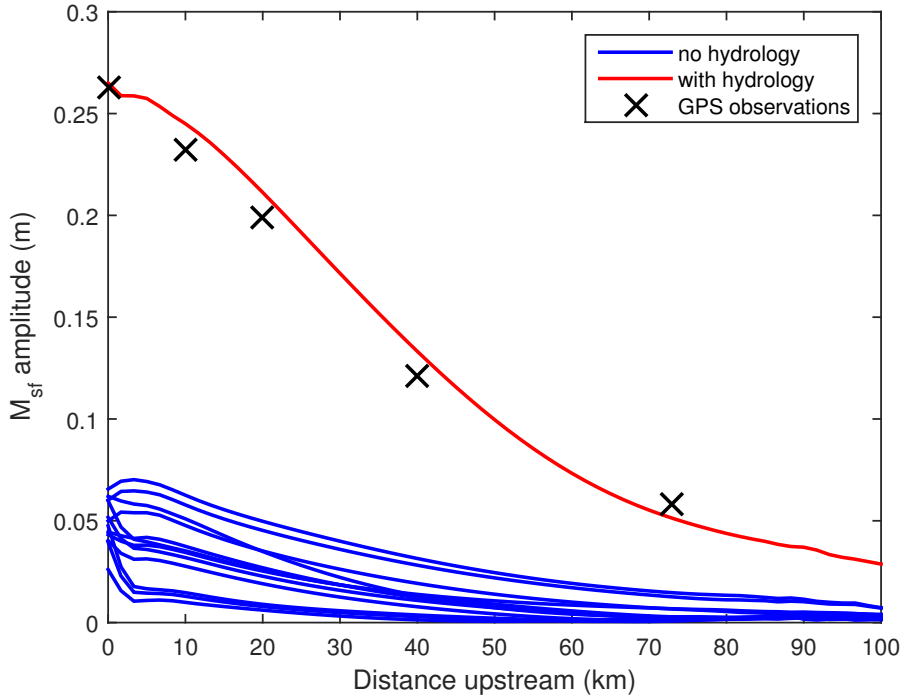

Figure 5. M_{sf} amplitude as a function of distance upstream for parameter study simulations with no hydrology (blue), compared with GPS measurements (crosses) and the best model fit using subglacial pressure variations (red).

TCD
9, 2397–2429, 2015

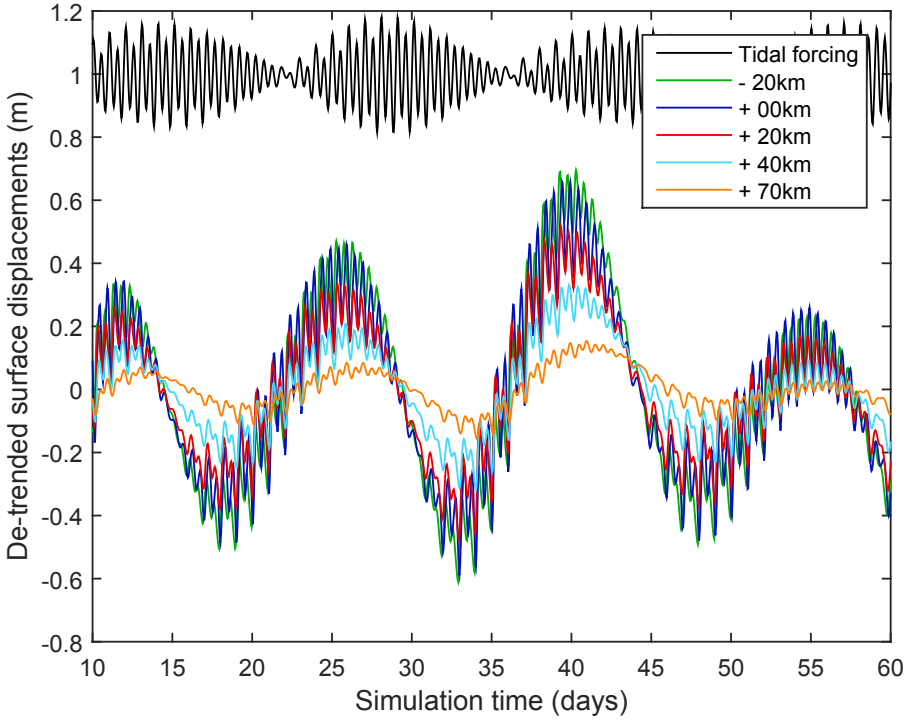

Figure 6. Modelled detrended horizontal surface displacements taken along the ice-stream medial at 20 km downstream (−20 km), at the grounding line (+00 km) and distances of 20, 40 and 70 km upstream of the grounding line (+20, +40 and +70 km respectively. The model was forced with $\overline{N}$ = 105 kPa, $K = 7 \times 10^9$ m^2 d^{-1}, q = 10, m = 3, E = 4.8 GPa and ν = 0.41.

TCD
9, 2397–2429, 2015

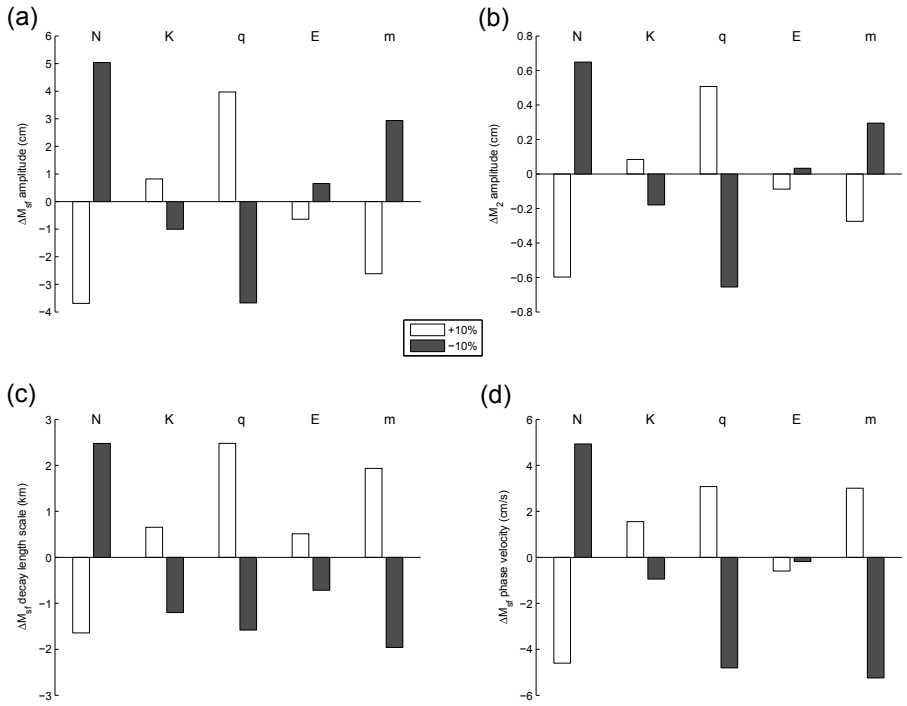

Figure 7. Sensitivity analysis of model parameters (N, K, q, E and m), showing change in M_{sf} and M_2 amplitudes (**a** and **b**), M_{sf} decay length scale **(c)** and M_{sf} phase velocity **(d)** for +10 % (white bar) and −10 % (grey bar) changes in each parameter. Model outputs were compared to the simulation presented in Fig. 6 and all other parameters were kept at the values defined in that plot.

TCD
9, 2397–2429, 2015

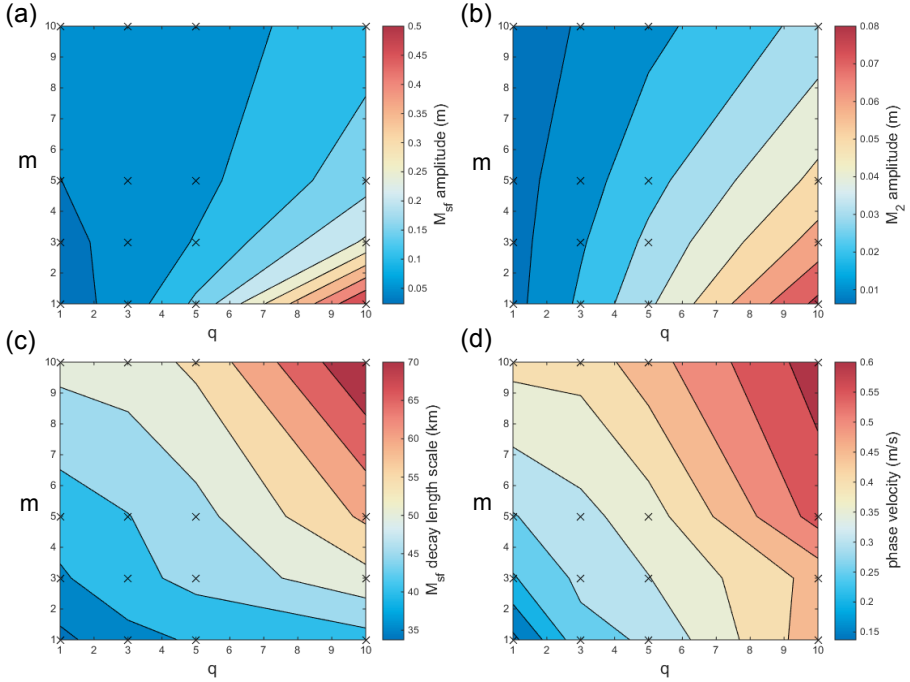

Figure 8. Response of M_{sf} amplitude **(a)**, M_2 amplitude **(b)**, M_{sf} decay length scale **(c)** and M_{sf} phase velocity **(d)** to choice of stress exponent (m) and hydrological exponent (q). Crosses indicate model simulations.

TCD
9, 2397–2429, 2015